Observing Electron Extraction by Monolayer Graphene Using Time-Resolved Surface Photoresponse Measurements

Lushuai Zhang,[†] Susmit Singha Roy,[†] Caroline R. English,[§] Robert J. Hamers,[†,§] Michael S. Arnold,[†] and Trisha L. Andrew*[,†,§]

[†]Department of Materials Science and Engineering and [§]Department of Chemistry, University of Wisconsin—Madison, Madison, Wisconsin 53706, United States

ABSTRACT Graphene is considered a next-generation electrode for indium tin oxide (ITO)-free organic photovoltaic devices (OPVs). However, to date, limited numbers of OPVs containing surface-modified graphene electrodes perform as well as ITO-based counterparts, and no devices containing a bare graphene electrode have been reported to yield satisfactory rectification characteristics. In this report, we provide experimental data to learn why. Time-resolved surface photoresponse measurements on templated pentacene-on-graphene films directly reveal that p-doped monolayer graphene efficiently extracts electrons, not holes, from photoexcited pentacene. Accordingly, a graphene/pentacene/MoO_3 heterojunction displays a large surface photoresponse and, by inference, efficient dissociation of photogenerated excitons, with graphene serving as an electron extraction layer and MoO_3 as a hole extraction layer. In contrast, a graphene/pentacene/C_{60} heterojunction yields a comparatively insignificant surface photoresponse because both graphene and C_{60} act as competing electron extraction layers. The data presented herein provide experimental insight for future endeavors involving bare graphene as an electrode for organic photovoltaic devices and strongly suggest that p-doped graphene is best considered a cathode for OPVs.

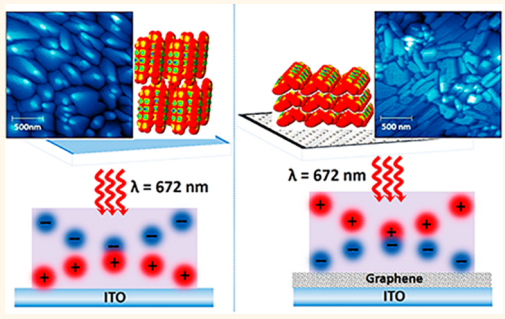

KEYWORDS: graphene · pentacene · charge extraction · surface photoresponse · built-in voltage

Indium tin oxide (ITO) is primarily used as a transparent conducting electrode for organic photovoltaic devices (OPVs).[1] However, ITO electrodes are not easily adaptable for flexible electronic devices due to poor tolerance for mechanical stress.[2] Further disadvantages, such as the limited elemental abundance of indium[3] and ion diffusion into organic active layers (which shortens device lifetime[4]), pose significant hindrances to developing next-generation OPVs for large-scale deployment.

Graphene is proposed as a viable alternative electrode due to its flexibility,[5] superior electrical conductivity (room-temperature carrier mobility ~20000 $cm^2\ v^{-1}\ s^{-1}$),[6] high optical transparency (only 2.3% of incident light absorbed in the range from near-infrared to violet),[5,7] and large-area processability.[8] Moreover, as a member of the 2D crystal family, high-quality graphene has minimal surface dangling bonds. As a result, reduced Shockley—Read—Hall recombination at graphene—organic semiconductor interfaces is expected due to the absence of trap states at the graphene interface.[9] Indeed, over the past half-decade, many attempts have been made to incorporate graphene into OPVs as either an anode or cathode.[2,5,10−16] Reported approaches involve tuning graphene conductivity,[11,16−18] work function,[19] and transparency and have met with limited success.[2] It was reported recently that surface engineering[12,13] of graphene leads to functional OPVs. In this case, spin coating PEDOT:PSS onto graphene allows its use as an anode, while depositing ZnO or TiO_x onto graphene allows its use as a cathode.[12,13]

However, none of the devices containing bare graphene (graphene without any surface modification) electrodes reported thus far show satisfactory diode characteristics, and the fundamental reason for this failure

* Address correspondence to tlandrew@wisc.edu.

Received for review September 8, 2014 and accepted March 8, 2015.

Published online March 09, 2015
10.1021/acsnano.5b01157

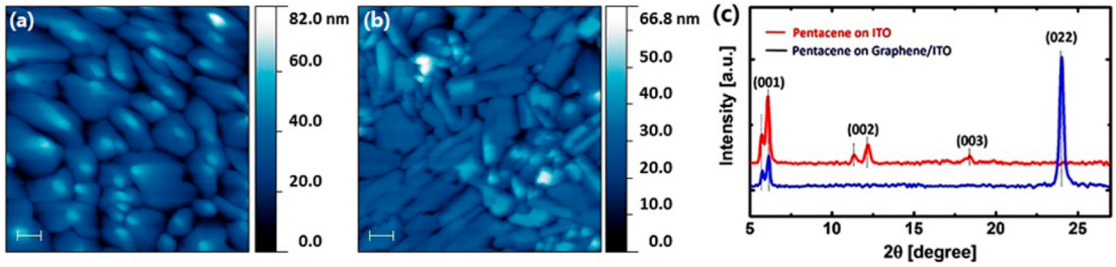

Figure 1. AFM topography images of a pentacene film grown on (a) bare ITO and (b) monolayer graphene-covered ITO. Scale bar = 200 nm. (c) X-ray diffraction (XRD) $\theta-2\theta$ scans of pentacene films on ITO and monolayer graphene-covered ITO. $2\theta = 5.71°$ and 6.15° represent the (001) phase of the pentacene crystal; $2\theta = 11.4°$, 12.2°, and 18.4° are corresponding higher order periodicities. $2\theta = 23.98°$ represents the (022) phase of the pentacene crystal.

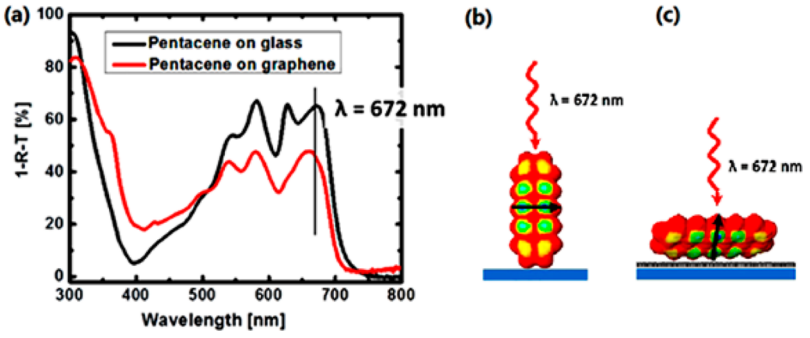

Figure 2. (a) %Absorption (1 − %*R* − %*T*) spectra of 300 nm thick pentacene grown on bare ITO and monolayer graphene-covered ITO. Bare ITO was used as a blank for the sample with and without graphene. The measured reflectance (%*R*) and transmittance (%*T*) spectra are provided in Figure S2 in the Supporting Information. The black line indicates the light absorbed by both samples at the excitation wavelength (λ = 672 nm) used in subsequent surface photoresponse studies. (b) Cartoon of standing-up pentacene on ITO with transition dipole moment (black arrow on the molecule) parallel to the substrate. (c) Cartoon of lying-down pentacene on graphene with transition dipole moment (black arrow on the molecule) forming an angle with the substrate.

remains unclear.[12,20] In this report, we detail direct experimental data with which to learn why. The surface photoresponse measurements discussed herein provide a guide for future endeavors involving bare graphene as an electrode, and we propose some viable strategies to use the attributes of graphene electrodes to bring large-area flexible OPVs into full play.

RESULTS AND DISCUSSION

Pentacene films of varying thickness were grown on ITO-coated glass, monolayer graphene supported on glass (graphene/glass), and monolayer graphene supported on ITO-coated glass (graphene/ITO) using physical vapor deposition. The morphologies and X-ray diffraction (XRD) spectra of physical vapor deposited pentacene films on ITO and graphene/ITO are shown in Figure 1. It was previously established that pentacene adopts a standing-up orientation on oxide surfaces and a lying-down orientation on graphene due to comparable van der Waals interactions between pentacene−graphene and pentacene−pentacene.[20] The pyramidal-like and plank-like crystal domains shown in Figure 1a and b depict the relative orientations of pentacene, consistent with previous studies.[20] The XRD data shown in Figure 1c confirm the crystal orientations relative to the substrate surface. The $\theta-2\theta$ scans of the pentacene film on bare ITO display Bragg peaks at 2θ = 5.71° and 6.15°, representing standing-up pentacene periodicity with $d_{(001)\ \text{thin film phase}}$ = 15.4 Å and $d_{(001)\ \text{bulk phase}}$ = 14.4 Å.[21,22] The $\theta-2\theta$ scan of the pentacene film on graphene/ITO shows a predominant Bragg peak at 2θ = 23.98°, representing a lying-down orientation of pentacene with $d_{(022)}$ = 3.7 Å,[20,23] and small peaks at 2θ = 5.71° and 6.15°, which are attributed to standing-up defects due to holes/tears in the graphene. Together, the AFM surface morphology images and XRD data confirm that pentacene adopts a standing-up orientation on bare ITO, while a majority of pentacene grains adopt a lying-down orientation on monolayer graphene, accompanied by a few defect regions of standing-up orientation.

The light absorbed by a 300 nm thick pentacene on either ITO or graphene/ITO was obtained by separately recording the reflectance (%*R*) and transmittance (%*T*) spectra and using the formula %*A* = 1 − %*R* − %*T* (see Figure 2 for the absorbance spectrum and Figure S1 in the Supporting Information for the separate reflectance and transmittance spectra). For 672 nm wavelength light, which is used in the surface photoresponse measurements described in this work, it is absorbed by pentacene on graphene/ITO lower than that absorbed by pentacene on bare ITO. As shown in

Figure 2b, the transition dipole moment of standing-up pentacene, which is in the direction of the short axis of the pentacene molecule,[24] is parallel to the substrate surface and also parallel to the electric field of the incident light. In the lying-down pentacene (Figure 2c), an angle exists between the pentacene transition dipole moment and the electric field vector of incoming light due to the tilt angle of the lying-down (022) orientation. Therefore, incident light is not absorbed as efficiently as when the electric field vector of incident light is parallel to the transition dipole moment of pentacene, as is the case with standing-up pentacene. As a result, the absorbance ($1 - \%T - \%R$) of lying-down pentacene on graphene/ITO is lower than that of standing-up pentacene on bare ITO.

Time-resolved surface photoresponse measurements were previously demonstrated to reveal the interfacial electronic properties of a heterojunction.[25] Typically this technique is used to study minority charge carriers in doped semiconductor heterojunctions in which a space charge region (SCR) is formed in the vicinity of a surface. The potential drop across this SCR drives photogenerated excitons to dissociate into free charge carriers that subsequently migrate to the surface to form a surface photovoltage. If a heterojunction interface is buried deep within the film or is otherwise inaccessible, the observed surface photoresponse will be attenuated or possibly inverted in sign because the energy bands in the semiconductor are serially connected. These two scenarios are classified as either surface dominated or buried interface dominated.[25,26]

In our experiment, the transient current induced by separation of charges at an organic heterojunction interface immediately after photoexcitation by a nanosecond optical pulse is measured at a capacitively coupled sense electrode, using a metal–insulator–semiconductor device architecture. The sample is grounded, and the sense electrode is connected through a voltage operational amplifier (op amp) to an oscilloscope (as shown in Figure S2). The impedance of the op amp and the oscilloscope are both 50 Ω. The instant surface charge generated upon illumination by a 3 ns laser pulse and its subsequent decay caused by recombination events are instantaneously sensed by the capacitively coupled sense electrode, which induces the charge to move from the sense electrode, through the op amp, to the oscilloscope. Thus, a current is produced and a voltage is built across the op amp based on Ohm's law, with 50 Ω resistance value. This voltage is amplified by 20 times during our measurement and is recorded. This recorded voltage is termed a "surface photoresponse" (V_{sp}). The surface photoresponse can be converted back to instantaneous charge (Q) using the following equations:

$$I = \frac{V_{sp}}{20 \times 50\Omega} \quad (1)$$

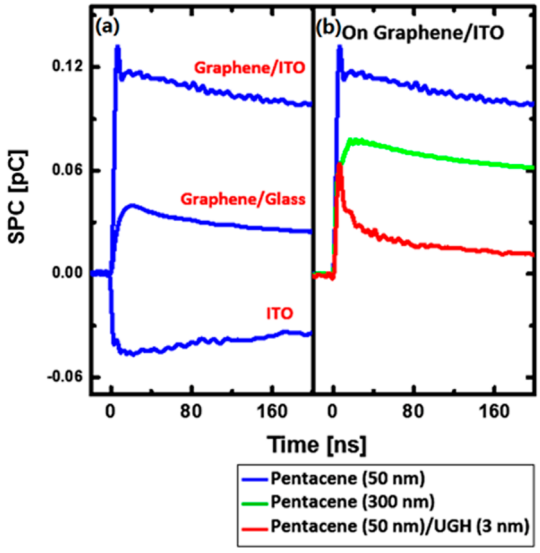

Figure 3. Surface photogenerated charge (SPC) *vs* time plots for various pentacene films. The instrumental setup is depicted in Figure S2. (a) 50 nm pentacene on ITO, graphene-covered glass (Graphene/Glass), or graphene-covered ITO (Graphene/ITO). (b) 50 nm pentacene (blue), 300 nm pentacene (green), and 50 nm pentacene capped with 3 nm UGH (red) on graphene/ITO.

$$Q = \int I \, dt \quad (2)$$

where 20 is the gain factor and 50 Ω is the input impedance of the op amp.

Integrating the recorded transient surface photoresponse *vs* time reveals the instantaneous values of surface photogenerated charge (SPC, measured in units of picocoulombs) obtained during the process of charge generation and decay. The maximum of this value provides a good measure of the overall charge generation efficiency of the heterojunction under study, which is related to the peak value of V_{sp}. Further, the surface charge decay can be fitted to a double-exponential function to reveal the lifetime of free charge carriers using the following equation:

$$\mathrm{SPV}(t) = y_0 + A_1 e^{-t/\tau_1} + A_2 e^{-t/\tau_2} \quad (3)$$

where y_0 is a y-axis offset, A_1 and A_2 are amplitude coefficients, τ_1 and τ_2 are decay constants, and t is the time in nanoseconds. One example of the measured surface photoresponse, the calculated instantaneous charge, and the fitting is shown in Figure S3.

Figure 3 shows surface photogenerated charge *vs* time curves obtained by integrating the measured surface photoresponse of 50 nm thick pentacene films on different substrates. The corresponding surface photoresponse curves are shown in Figure S4. Figure 3a shows the surface photogenerated charge for pentacene films on ITO, graphene/ITO, and graphene/glass. A negative sign of the transient signal was observed for pentacene on ITO, as expected, due to electron accumulation at the pentacene–air interface.

Observing electron accumulation at the pentacene–air interface is expected because the surface photoresponse technique probes minority carriers, which are electrons for a p-type organic semiconductor such as pentacene, and because ITO provides electronic states for hole accumulation at the ITO–pentacene interface, meaning that electrons will accumulate at the pentacene–air interface. In stark contrast, pentacene films grown on monolayer graphene supported on glass or on ITO displayed *positive* transient signal values, indicating hole accumulation at the pentacene–air interface and electron accumulation at the pentacene–graphene interface. Additionally, comparing pentacene films grown on graphene/ITO and on bare ITO, the absolute value of the charge accumulation is also 3 times higher for the sample with graphene. This difference in charge generation efficiency cannot be attributed to an optical effect: as discussed above (Figure 2a), the light absorbed at 672 nm by pentacene on graphene/ITO is lower than that absorbed by pentacene on ITO, which should nominally reduce the magnitude of the observed photoresponse transient for pentacene on graphene/ITO. Indeed, these observations are a direct measurement of the significant electronic effect of graphene on pentacene.

Figure 3b shows the effect of film thickness and surface encapsulation on the surface photogenerated charge on pentacene film grown on graphene/ITO. The photogenerated charge reduces from 0.13 pC (blue) to 0.07 pC (green) when the thickness of the pentacene film is increased from 50 to 300 nm. Considering the exciton diffusion length under 672 nm illumination (65 nm),[27] reduced charge accumulation for thicker samples is expected due to a higher incidence of exciton recombination in thicker films if a major portion of charge is generated at the buried interface, away from the surface. This confirms that the graphene–pentacene interface dominates the observed surface charge accumulation.

The surface photoresponse of a 50 nm pentacene film encapsulated with a 3 nm thick layer of *m*-bis(triphenylsilyl)benzene (UGH3) was also measured. UGH3 is a wide-band-gap semiconductor and does not have appropriate band-edge alignment with pentacene to extract either electrons or holes at the UGH3/pentacene interface. Therefore, a 3 nm UGH3 layer will effectively block charge carriers within the pentacene layer from reaching the surface, although some charges are still expected to tunnel through 3 nm of UGH3 to reach the surface. Overall, a decreased accumulation of charges at the pentacene surface can be expected for UGH3-capped samples compared to samples without a UGH3 capping layer. Indeed, a positive signal is also observed for 50 nm pentacene on graphene/ITO with a UGH3 cap (Figure 3b, red), but the observed surface charge value is decreased to 0.06 pC. Overall, this encapsulation experiment allows us to confirm that the transient surface photoresponse measurement used in this report is exquisitely sensitive to the surface environment.

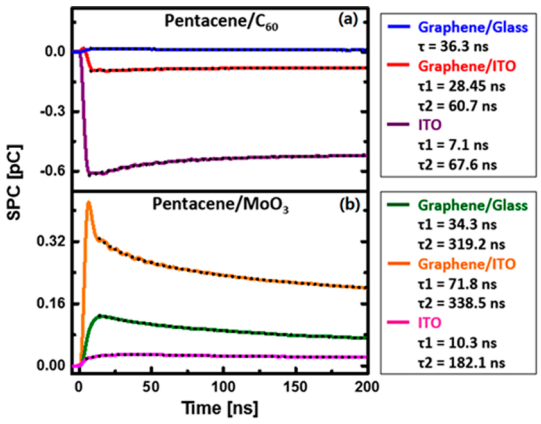

Figure 4. Surface photogenerated charge (SPC) *vs* time plots for various pentacene-containing heterojunctions on ITO, graphene/glass, or graphene/ITO. (a) Pentacene (50 nm)/C_{60} (40 nm). (b) Pentacene (50 nm)/MoO_3 (20 nm).

We also investigated the transient surface charge generated in various pentacene-containing donor–acceptor heterojunctions (Figure 4). All corresponding measured surface photoresponse curves are provided in Figure S5 of the Supporting Information. The transient surface charge generated in these incomplete circuits reflects the expected open-circuit voltage (V_{oc}) of the corresponding diodes with or without graphene. Photogenerated excitons are expected to dissociate at the donor–acceptor interface and yield free charges, which will build up the quasi Fermi level difference between the donor and acceptor materials. This quasi Fermi level difference essentially determines the V_{oc} of the corresponding complete diode under illumination. We note that, in this experiment, only pentacene was excited upon illumination with a single wavelength (λ = 672 nm) of weak excitation fluence (0.1 mJ), and therefore, the expected value of V_{oc} is much lower than that expected for corresponding photovoltaic devices illuminated under 1 sun.

Figure 4a shows the surface photogenerated charge of a pentacene/C_{60} heterojunction grown on ITO, graphene/glass, and graphene/ITO. The negative signal of the photogenerated surface charge (−0.62 pC) of the heterojunction on bare ITO is consistent with the injection of electrons from the excited pentacene molecules into the C_{60}. However, the same pentacene/C_{60} heterojunction on graphene/ITO shows a significantly decreased negative transient surface charge (−0.091 pC), and a small positive transient surface charge (+0.018 pC) is observed for the same heterojunction on graphene/glass. This observation strongly suggests that electron extraction is dominant at the pentacene/graphene interface. Electrons are extracted at both the pentacene/graphene and

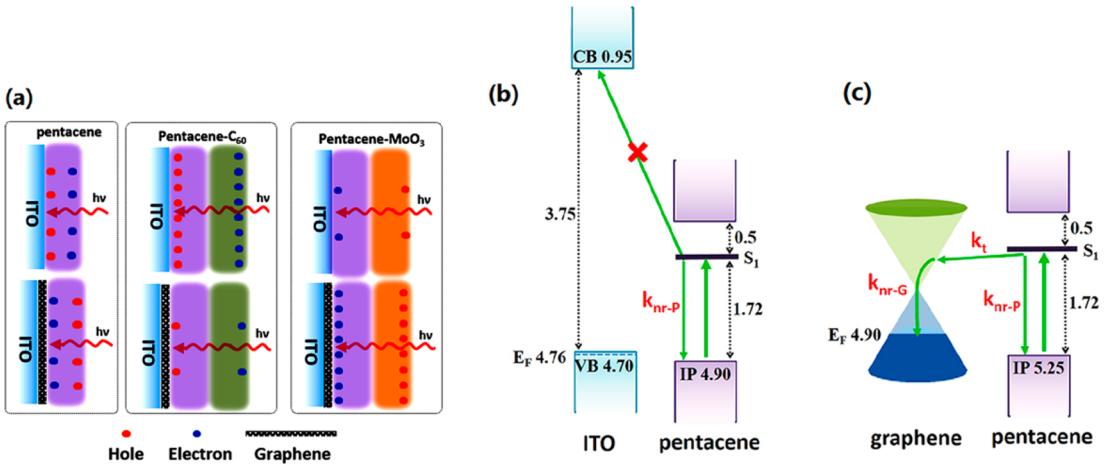

Figure 5. (a) Cartoons detailing transient charge accumulation upon photoexcitation for each film or heterojunction. (b) Energy diagram of graphene and pentacene, showing both the band edges and first singlet excitonic state of pentacene. (c) Proposed mechanism of efficient photoexcited electron transfer from pentacene to graphene.

pentacene/C_{60} interfaces, effectively deteriorating the built-in voltage typically found in pentacene/C_{60} heterojunctions, which explains why most diodes incorporating a naked graphene anode (graphene without a hole injection layer) display poor to zero rectification.[12,20]

To properly capitalize on the electronic effect of graphene, an inverse diode was constructed: ITO or glass/graphene/pentacene (50 nm)/MoO_3 (20 nm), where MoO_3 was predicted to act as an efficient hole extraction layer. An analogous control device was also constructed, excluding the graphene layer: ITO/pentacene (50 nm)/MoO_3 (20 nm). The integrated instantaneous surface charge is shown in Figure 4b. As expected, a large positive transient surface charge (+0.42 pC) was observed for the ITO/graphene/pentacene/MoO_3 sample, followed by the glass/graphene/pentacene/MoO_3 sample (0.13 pC), while the control graphene-free heterojunction shows a negligible surface charge (0.021 pC). The accumulation of holes at the surface of MoO_3 on ITO or glass/graphene/pentacene is bolstered by efficient electron extraction at the lying-down pentacene/graphene interface and hole extraction at the pentacene/MoO_3 interface. It was previously established that a large density of gap states renders MoO_3 an efficient hole extraction material for most organic optoelectronic devices;[28] therefore, we can effectively ignore the seemingly large hole extraction barrier between pentacene of various intermolecular orientations and MoO_3.

The lifetimes of surface charges for various pentacene heterojunctions are also shown in Figure 4. We are more interested in τ_2, the slow decay component, since the fast decay component, τ_1, is comparatively sensitive to instrumental artifacts. We observed that τ_2 is dependent on the type of surface charge. For pentacene/C_{60} heterojunctions on ITO or graphene/ITO, electrons accumulate at the C_{60} surface, and similar τ_2 values, 67.6 and 60.7 ns, were observed. In contrast, holes accumulated at the C_{60} surface for pentacene/C_{60} heterojunctions on graphene/glass, and a single component decay curve was obtained with τ = 36.3 ns. For the pentacene/MoO_3 heterojunction, close τ_2 values of 319.2 and 338.5 ns were observed for samples on graphene/ITO and graphene/glass, accompanied by significant hole accumulation at the MoO_3 surface. For samples on ITO, which displayed a negligible amount of hole accumulation, an average τ_2 value of 182.1 ns was observed. These results further confirm that graphene plays a significant role in electron extraction in heterojunctions with appropriate band-edge alignment and is able to increase charge lifetime.

The charge accumulation behavior upon photoexcitation of the neat pentacene films and the heterojunctions is summarized in Figure 5a. Figure 5b and c depicts the energy band diagram, including excitonic states (S_1), of our pentacene—ITO and pentacene—graphene interface and details our proposed driving force for hole accumulation at the pentacene surface in samples containing graphene. The p-doped graphene used in study has a work function of 4.90 eV, and ITO has a work function of 4.76 eV (measured by calibrated Kelvin probe force microscopy). It is known that ITO has a large band gap (>3.75 eV).[29] The energy levels of ITO valence band (VB 4.70 eV) and conduction band (CB 0.95 eV) and the ionization potentials of lying-down pentacene (5.25 eV) and standing-up pentacene (4.90 eV) are extracted from previously reported studies.[30,31] A large exciton binding energy (*ca.* 0.5 eV) was previously measured for pentacene films.[32] The optical band gap of pentacene (1.72 eV) was obtained from its absorption onset (Figure 2). Standing-up pentacene (IP 4.90 eV) encounters a hole injection barrier (HIB) of 0.14 eV at an ITO interface (ϕ 4.76 eV), whereas lying-down pentacene (IP 5.25) experiences a HIB of

0.35 eV at the p-doped graphene interface (ϕ 4.90 eV). Thus, the deeper IP of lying-down pentacene introduces a larger HIB, here 0.21 eV larger on p-doped graphene than on ITO. Besides the larger HIB, another significant factor is the large density of empty states introduced by graphene. Photoexcited electron transfer from pentacene to graphene experiences no energy barrier due to the presence of a large density of empty graphene states near the pentacene first singlet excitonic state. As long as the rate of photoexcited electron transfer from pentacene to graphene (k_t) and nonradiative decay in graphene ($k_{nr\text{-}G}$) are, in combination, greater than the rate of nonradiative decay of the pentacene exciton ($k_{nr\text{-}PEN}$), *i.e.*, when $(1/k_t + 1/k_{nr\text{-}G}) \ll 1/k_{nr\text{-}PEN}$, then electron extraction at the pentacene–graphene interface will be facile and efficient, as shown in Figure 5c.[33] In contrast, ITO lacks available states near the pentacene first singlet excitonic state due to its large band gap, so photoexcited electron transfer from pentacene to ITO is negligible. As a result, under 672 nm illumination, ITO/pentacene displays electron accumulation at the pentacene surface with holes injected into ITO, while graphene/pentacene has significant hole accumulation at the pentacene surface due to efficient electron injection into graphene.

CONCLUSIONS

Ordered pentacene films grown on monolayer graphene are suitable for direct transformation to ITO-free optoelectronic devices, such as photovoltaic cells, with the added possible benefit of graphene serving as a diffusion barrier to improve device stability. Time-resolved surface photoresponse measurements were recorded for pentacene films of varying thickness grown on bare ITO, monolayer graphene-covered glass, or monolayer graphene-covered ITO. As expected, electron accumulation was observed at the pentacene–air interface for films grown directly on ITO, while unexpectedly, hole accumulation was observed at the pentacene–air interface for films grown on graphene/glass or graphene/ITO, indicating that graphene preferentially extracts electrons from pentacene. To support this hypothesis, the surface photoresponse of a pentacene/MoO_3 heterojunction was measured, with the expectation that adding an efficient hole-extracting MoO_3 layer away from the graphene/pentacene interface will increase the magnitude of the observed surface charge. Indeed, the pentacene/MoO_3 heterojunction displayed significantly larger surface charge values and increased charge carrier lifetimes with graphene than without graphene. This result is especially significant, considering that a typical graphene/pentacene/C_{60} heterojunction yielded a comparatively insignificant surface photoresponse and low charge carrier lifetimes, suggesting that a pentacene/C_{60} photoactive layer will perform poorly as a photovoltaic device if the pentacene is electrically contacted to a bare graphene anode. Our surface photoresponse measurements empirically confirm that graphene is best considered as a potential cathode for OPVs, as previously suggested in the literature.[12]

EXPERIMENTAL METHODS

Pentacene films were prepared by thermal evaporation of source material (TCI sublimed grade) onto monolayer graphene, O_2 plasma treated ITO with chamber pressures below 1×10^{-6} Torr and a deposition rate of 0.3 Å/s. The film crystallinity and orientation were characterized using a Bruker D8 Discovery X-ray diffractometer in the θ–2θ configuration with a Cu Kα (wavelength = 1.542 Å) source and 0.5 mm slit width. Absorption spectra of all films were recorded using an Evolution 220 UV–visible spectrophotometer with an ISA 220 integrating sphere under reflectance and transmittance mode.

CVD Graphene Growth. Monolayers of graphene were grown on Cu foils (Alfa Aesar product 13382, lot B03Y027) as the growth catalyst. The foils were precleaned with acetic acid (Fisher) for 15 min to remove contaminants and native oxides, then rinsed in DI water three times before being dried with an air-gun. The cleaned Cu foils were then annealed for 30 min at 1030 °C in 95% argon + 5% hydrogen (340 sccm flow rate) to remove trace surface contaminants and also to reduce the surface roughness of the foil before initiating the growth process. The growth was conducted at 1030 °C with 95% argon + 5% methane (0.300 sccm) and 95% argon + 5% hydrogen (340 sccm) for 3 h. The manufactured graphene on Cu foils was stored in a N_2 glovebox to minimize the oxidation of the graphene and the copper surfaces.

Graphene Transfer. Graphene monolayers grown *via* CVD were transferred onto 150 nm thick ITO on glass substrates. The transfer was completed using a sacrificial polymer (poly(methyl methacrylate), PMMA), similar to previous reports.[34,35] CVD-graphene on copper was overcoated with PMMA (MW = 925k, 2% in chlorobenzene) by spin-coating at 2000 rpm. The samples were placed in copper etchant 0.2 M ammonium persulfate (APS) and then bath-ultrasonicated for 15 min to remove the bottom-facing graphene layer. The samples were left overnight (10 h) in the etchant for the copper to completely etch. Postetch, the floating PMMA on graphene was scooped out from the APS solution and refloated in DI water three times to rinse any residual copper etchant. The samples were then floated in 5% HF in DI water for 60 min to remove trace silica particles that might have deposited from the CVD system during graphene growth, following which they were rinsed in DI water three times. From the final DI water bath, the samples were scooped on to glass or ITO-coated glass and spin-dried at 8000 rpm for 2 min to remove water trapped between the graphene sheet and the substrate. To remove the PMMA layer, the samples were placed in room-temperature acetone baths twice for 20 min, after which they were rinsed in 2-propanol for 2 min to wash away any residual acetone. Finally, they were dried using an air gun and then annealed in an Ar atmosphere for 2 h at 500 °C to remove any residual PMMA. The Ar anneal step was found to be very critical, as it resulted in more atomically pristine graphene surfaces more analogous to freshly cleaved HOPG.

Kelvin Probe Force Microscopy (KPFM). KPFM is a noncontact technique that maps the contact potential difference (CPD) of a sample, concomitant with topography. CPD is defined as

$$\mathrm{CPD}_{\mathrm{sample}} = (\varphi_{\mathrm{tip}} - \varphi_{\mathrm{sample}})/e \quad (4)$$

where ϕ_{tip} and ϕ_{sample} are the work functions of the conductive tip and sample, respectively, and e is elementary charge.

An Agilent 5500 atomic force microscope was used for this KPFM study. The work function of the tip (NSC18/Pt coated, 75kHZ, 2.8 N/m, Mikromasch USA) was first calibrated by scanning a freshly cleaved highly ordered pyrolytic graphite (HOPG) sample with known work function. Scans were performed in a single-scan amplitude mode, in which the topography and CPD images were obtained simultaneously. Amplitude mode (AM) was chosen because it yielded 25 nm spatial resolution and 5 meV energy resolution. AFM and KPFM data were analyzed using Gwyddion.[36] See Figure S6.

Surface Photoresponse Measurements. The experimental setup is shown is Figure S2. Surface photoresponse measurements were performed with custom-built ultrafast electronics (with nanosecond resolution) using a metal−insulator−semiconductor device architecture. In a typical device, the sample film (*e.g.*, pentacene or graphene-pentacene) served as the semiconductor and was deposited on ITO, which served as the back electrode. The insulator was a 127 μm air gap, achieved using a Teflon spacer. A second ITO-on-glass slide served as the transparent front (sense) electrode. A tunable pulsed laser (NT340, EKSPA, Inc., Vilnius, Lithuania) was used to illuminate samples through the front sense electrode at a maximum incident power of 0.1 mJ and 0.2 mJ/pulse with 3 ns duration. The surface photoresponse was recorded as a voltage change using a digital oscilloscope (model DSO9404A, Agilent, Inc., Santa Clara, CA, USA) with 50 Ω input impedance. The recorded voltage is not a *direct* measure of the surface photovoltage generated in the device, but is a measure of the change in the capacitance of the full circuit (device, oscilloscope, and op amp); this recorded voltage is therefore termed a "surface photoresponse" for accuracy.

Conflict of Interest: The authors declare no competing financial interest.

Supporting Information Available: Transmittance and reflectance spectra of pentacene films. This material is available free of charge *via* the Internet at http://pubs.acs.org.

Acknowledgment. The authors gratefully acknowledge support from the University of Wisconsin Materials Research Science and Engineering Center (DMR-1121288). Partial support is acknowledged by M.S.A. and S.S.R. for graphene synthesis and transfer, from the National Science Foundation (Grant Number CBET-1033346) and the DOE Office of Science Early Career Research Program (Grant Number DE-SC0006414) through the Office of Basic Energy Sciences. We thank Prof. Song Jin for providing access to his AFM.

REFERENCES AND NOTES

1. Cao, W.; Xue, J. Recent Progress in Organic Photovoltaics: Device Architecture and Optical Design. *Energy Environ. Sci.* **2014**, *7*, 2123–2144.
2. De Arco, L. G.; Zhang, Y.; Schlenker, C. W.; Ryu, K.; Thompson, M. E.; Zhou, C. Continuous, Highly Flexible, and Transparent Graphene Films by Chemical Vapor Deposition for Organic Photovoltaics. *ACS Nano* **2010**, *4*, 2865–2873.
3. Jaffe, R.; Price, J.; Ceder, G.; Eggert, R.; Graedel, T.; Gschneidner, K.; Hitzman, M.; Houle, F.; Hurd, A.; Kelley, R. *et al. Energy Critical Elements: Securing Materials for Emerging Technologies*; Technical Report for APS Panel on Public Affairs; Warrendale, PA, February **2011**.
4. Li, Y.; Liu, C.; Tong, S.; Pan, L.; Pu, L.; Minari, T.; Tsukagoshi, K.; Shi, Y. Metal-Diffusion-Induced ITO Nanoparticles at the Organic/ITO Interface. *J. Phys. D Appl. Phys.* **2012**, *45*, 165104.
5. Liu, Z.; Li, J.; Yan, F. Package-Free Flexible Organic Solar Cells with Graphene Top Electrodes. *Adv. Mater.* **2013**, *25*, 4296–4301.
6. Chen, J. H.; Jang, C.; Xiao, S.; Ishigami, M.; Fuhrer, M. S. Intrinsic and Extrinsic Performance Limits of Graphene Devices on SiO_2. *Nat. Nanotechnol.* **2008**, *3*, 206–209.
7. Nair, R. R.; Blake, P.; Grigorenko, A. N.; Novoselov, K. S.; Booth, T. J.; Stauber, T.; Peres, N. M. R.; Geim, A. K. Fine Structure Constant Defines Visual Transparency of Graphene. *Science* **2008**, *320*, 1308.
8. Bae, S.; Kim, H.; Lee, Y.; Xu, X.; Park, J.-S.; Zheng, Yi.; Balakrishnan, J.; Lei, T.; Kim, H. R.; Song, Y. I.; *et al.* Roll-to-Roll Production of 30-inch Graphene Films for Transparent Electrodes. *Nat. Nanotechnol.* **2010**, *5*, 574–578.
9. Hong, X.; Kim, J.; Shi, S.-F.; Zhang, Y.; Jin, C.; Sun, Y.; Tongay, S.; Wu, J.; Zhang, Y.; Wang, F. Ultrafast Charge Transfer in Atomically Thin MoS2/WS2 Heterostructures. *Nat. Nanotechnol.* **2014**, *9*, 682–686.
10. Bi, H.; Huang, F.; Liang, J.; Xie, X.; Jiang, M. Transparent Conductive Graphene Films Synthesized by Ambient Pressure Chemical Vapor Deposition Used as the Front Electrode of CdTe Solar Cells. *Adv. Mater.* **2011**, *23*, 3202–3206.
11. Hsu, C.-L.; Lin, C.-T.; Huang, J.-H.; Chu, C.-W.; Wei, K.-H.; Li, L.-J. Layer-by-Layer Graphene/TCNQ Stacked Films as Conducting Anodes for Organic Solar Cells. *ACS Nano* **2012**, *6*, 5031–5039.
12. Park, H.; Chang, S.; Smith, M.; Gradečak, S.; Kong, J. Interface Engineering of Graphene for Universal Applications as Both Anode and Cathode in Organic Photovoltaics. *Sci. Rep.* **2013**, *3*, 1581.
13. Park, H.; Kong, J. An Alternative Hole Transport Layer for Both ITO- and Graphene-Based Organic Solar Cells. *Adv. Energy Mater.* **2014**, *4*, 1301280.
14. Wang, Y.; Tong, S. W.; Xu, X. F.; Ozyilmaz, B.; Loh, K. P. Interface Engineering of Layer-by-Layer Stacked Graphene Anodes for High-Performance Organic Solar Cells. *Adv. Mater.* **2011**, *23*, 1514–1518.
15. Yin, Z.; Zhu, J.; He, Q.; Cao, X.; Tan, C.; Chen, H.; Yan, Q.; Zhang, H. Graphene-Based Materials for Solar Cell Applications. *Adv. Energy Mater.* **2014**, *4*, 1300574.
16. Qu, S.; Li, M.; Xie, L.; Huang, X.; Yang, J.; Wang, N.; Yang, S. Noncovalent Functionalization of Graphene Attaching [6,6]-Phenyl-C61-Butyric Acid Methyl Ester (PCBM) and Application as Electron Extraction Layer of Polymer Solar Cells. *ACS Nano* **2013**, *7*, 4070–4081.
17. Kim, K.; Bae, S. H.; Toh, C. T.; Kim, H.; Cho, J. H.; Whang, D.; Lee, T. W.; Ozyilmaz, B.; Ahn, J. H. Ultrathin Organic Solar Cells with Graphene Doped by Ferroelectric Polarization. *ACS Appl. Mater. Interfaces* **2014**, *6*, 3299–3304.
18. Kim, K. K.; Reina, A.; Shi, Y.; Park, H.; Li, L. J.; Lee, Y. H.; Kong, J. Enhancing the Conductivity of Transparent Graphene Films *via* Doping. *Nanotechnology* **2010**, *21*, 285205.
19. Shi, Y.; Kim, K. K.; Reina, A.; Hofmann, M.; Li, L.-J.; Kong, J. Work Function Engineering of Graphene Electrode *via* Chemical Doping. *ACS Nano* **2010**, *4*, 2689–2694.
20. Berke, K.; Tongay, S.; McCarthy, M. A.; Rinzler, A. G.; Appleton, B. R.; Hebard, A. F. Current Transport Across the Pentacene/CVD-Grown Graphene Interface for Diode Applications. *J. Phys.: Condens. Matter* **2012**, *24*, 255802.
21. Drummy, L. F.; Miska, P. K.; Martin, D. C. Crystal Structure of and Defects in the Pentacene Thin Film Phase. *Mater. Res. Soc. Symp. Proc.* **2003**, *734*, A.2.2.1–A.2.2.5.
22. Mattheus, C. C.; Dros, A. B.; Baas, J.; Oostergetel, G. T.; Meetsma, A.; de Boer, J. L.; Palstra, T. T. M. Identification of Polymorphs of Pentacene. *Synth. Met.* **2003**, *138*, 475–481.
23. Götzen, J.; Käfer, D.; Wöll, C.; Witte, G. Growth and Structure of Pentacene Films on Graphite: Weak Adhesion as a Key for Epitaxial Film Growth. *Phys. Rev. B* **2010**, *81*, 085440.
24. Tiago, M. L.; Northrup, J. E.; Louie, S. G. *Ab Initio* Calculation of the Electronic and Optical Properties of Solid Pentacene. *Phys. Rev. B* **2003**, *67*, 115212.
25. Kronik, L.; Shapira, Y. Surface Photovoltage Phenomena: Theory, Experiment, and Applications. *Surf. Sci. Rep.* **1999**, *37*, 1–206.
26. Kronik, L.; Shapira, Y. Surface Photovoltage Spectroscopy of Semiconductor Structures: At the Crossroads of Physics, Chemistry and Electrical Engineering. *Surf. Interface Anal.* **2001**, *31*, 954–965.
27. Yoo, S.; Domercq, B.; Kippelen, B. Efficient Thin-Film Organic Solar Cells Based on Pentacene/C_{60} Heterojunctions. *Appl. Phys. Lett.* **2004**, *85*, 5427.
28. Hancox, I.; Sullivan, P.; Chauhan, K. V.; Beaumont, N.; Rochford, L. A.; Hatton, R. A.; Jones, T. S. The Effect of a

MoOx Hole-Extracting Layer on the Performance of Organic Photovoltaic Cells Based on Small Molecule Planar Heterojunctions. *Org. Electron.* **2010**, *11*, 2019–2025.
29. Balasubramanian, N.; Subrahmanyam, A. Electrical and Optical Properties of Reactively Evaporated Indium Tin Oxide (ITO) Films Dependence on Substrate Temperature and Tin Concentration. *J. Phys. D Appl. Phys.* **1989**, *22*, 206–209.
30. Méndez-Pinzón, H. A.; Pardo-Pardo, D. R.; Cuéllar-Alvarado, J. P.; Salcedo-Reyes, J. C.; Vera, R.; Páez-Sierra, B. A. Analysis of the Current-Voltage Characteristics of Polymer-Based Organic Light-Emitting Diodes (OLEDs) Deposited by Spin Coating. *Univ. Sci.* **2010**, *15*, 68–76.
31. Liu, X.; Grüneis, A.; Haberer, D.; Fedorov, A. V.; Vilkov, O.; Strupinski, W.; Pichler, T. Tunable Interface Properties between Pentacene and Graphene on the SiC Substrate. *J. Phys. Chem. C* **2013**, *117*, 3969–3975.
32. Sharifzadeh, S.; Biller, A.; Kronik, L.; Neaton, J. B. Quasiparticle and Optical Spectroscopy of the Organic Semiconductors Pentacene and PTCDA from First Principles. *Phys. Rev. B* **2012**, *85*, 125307.
33. Shim, G. W.; Yoo, K.; Seo, S.-B.; Shin, J.; Jung, D. Y.; Kang, I.-S.; Ahn, C. W.; Cho, B. J.; Choi, S.-Y. Large-Area Single-Layer $MoSe_2$ and its van der Waals Heterostructures. *ACS Nano* **2014**, *8*, 6655–6662.
34. Li, X.; Zhu, Y.; Cai, W.; Borysiak, M.; Han, B.; Chen, D.; Piner, R. D.; Colombo, L.; Ruoff, R. S. Transfer of Large-Area Graphene Films for High-Performance Transparent Conductive Electrodes. *Nano Lett.* **2009**, *9*, 4359–4363.
35. Singha Roy, S.; Bindl, D. J.; Arnold, M. S. Templating Highly Crystalline Organic Semiconductors Using Atomic Membranes of Graphene at the Anode/Organic Interface. *J. Phys. Chem. Lett.* **2012**, *3*, 873–878.
36. Nečas, D.; Gwyddion, P. K. An Open-Source Software for SPM Data Analysis. *Cent. Eur. J. Phys.* **2012**, *10*, 181–188.